NURETH14-204

FLUID FLOW AND HEAT TRANSFER INVESTIGATION OF PEBBLE BED REACTORS USING MESH ADAPTIVE LARGE-EDDY SIMULATION

D. Pavlidis and D. Lathouwers

Section Physics of Nuclear Reactors Delft University of Technology, Delft, The Netherlands

Abstract

A computational fluid dynamics model with anisotropic mesh adaptivity is used to investigate coolant flow and heat transfer in pebble bed reactors. A novel method for implicitly incorporating solid boundaries based on multi-fluid flow modelling is adopted. The resulting model is able to resolve and simulate flow and heat transfer in randomly packed beds, regardless of the actual geometry, starting off with arbitrarily coarse meshes. The model is initially evaluated using an orderly stacked square channel of channel-height-to-particle diameter ratio of unity for a range of Reynolds numbers. The model is then applied to the face-centred cubical geometry. Coolant flow and heat transfer patterns are investigated.

Introduction

Optimal design and safe operation of pebble bed reactors necessitates the investigation of coolant flow and heat transfer at the microscopic level. Physical experiments have been performed to investigate packing, flow fields and to some extent heat transfer in these complex geometries (for example see [1-3]). However, these experiments are best suited for evaluation purposes of numerical models. The latter can then be used more efficiently in the detailed study of transport phenomena in such environments. The majority of these numerical studies are concerned with modelling either a 'unit cell' which includes a small number of particles, or part of the bed using as many particles as possible. A brief review of the most fundamental ones is given here.

As far as unit cell studies are concerned, Dalman et al. [4], Kuwahara et al. [5-7], Pedras and de Lemos [8] and Nakayama and Kuwahara [9] used 2D computational domains to investigate fluid flow and heat transfer, and derive macroscopic correlations for packed beds.

As far as more complex geometry studies are concerned, Tobiś [10] modelled a simple cubical (SC) stacking unit cell (aligned with a central cavity) and introduced a turbulence promoter in the geometry cavity. It was confirmed that the bed porosity and the hydraulic diameter were not sufficient to describe properly the hydrodynamic properties of randomly packed beds.

Gunjal et al. [11] used SC, face-centred cubical (FCC) and rhombohedral unit cells to investigate drag forces, flow patterns and Nusselt (*Nu*) numbers.

Logtenberg and Dixon [12] modelled a 3D geometry of 8 pseudo-randomly stacked spheres in a cylindrical channel with inter-pebble and channel-pebble gaps. The wall heat transfer coefficient, Nu number and the radial effective thermal conductivity ratio were investigated. This work was

later extended to include contact points between solid surfaces [13]. Nijemeisland and Dixon [14] used a 3D geometry of 44 pseudo-randomly stacked spheres. However, due to numerical issues, inter-pebble contact points were eliminated and spheres were shrunk by 1%. Finally, Dixon and Nijemeisland [15] used a 3D geometry of pseudo-randomly stacked spheres with different channel-to-particle ratios (*N*).

Calis et al. [16] modelled a 3D geometry of pseudo-randomly stacked spheres with N ranging from 1 to 2 using 8-16 spheres for Reynolds (Re) numbers between 0.01 and 5,000. Pressure drops were compared against experimental data. Particles were shrunk by 1% to avoid interpebble contact points. Romkes et al. [17] extended Calis et al.'s work to incorporate heat transfer. Results (mainly Nu numbers) were compared against experimental data with good agreement. Experimental Nu numbers were obtained by replacing one or more spheres in the packing by spheres made of naphthalene, and determining the rate of mass decrease of the naphthalene spheres.

Guardo et al. [18] modelled a 3D geometry of 44 randomly stacked spheres in a cylindrical channel. The spheres overlapped by increasing their diameter by 1%. The *Nu* number, pressure drop and radial effective thermal conductivity ratio were investigated.

Lee et al. [19], initially, investigated the influence of inter-pebble gaps by simulating flow past two spheres at various relative distances. It was concluded that approximate gaps could give inaccurate information about the local flow fields, in spite of their advantages (simplification of calculation and mesh generation). The model was then applied to the body-centred cubical (BCC) stacking (with 1mm inter-pebble gaps and contact areas). It was suggested that, more accurate results would be expected if direct contacts among the pebbles were used.

Lee et al. [20], initially, modelled flow past a cylinder using large-eddy simulation (LES) and a large number of RANS-based models to investigate flow and temperature patterns. The two best performing turbulence models (LES and k- ω) were then used for the FCC and BCC stackings with 1mm inter-pebble gaps. LES and k- ω results were not comparable and it was concluded that LES was better in predicting turbulence-induced heat transfer.

Hassan [21] modelled a 3 pebble diameter long BCC stacking (24 pebbles in total) using a Smagorinsky-based LES model and inter-pebble contact points. Velocity, pressure and pebble surface temperature distributions were investigated.

Kim et al. [22] modelled 5 pebble diameter long SC, FCC and BCC stackings. Heat transfer was modelled within the solids. A 0.5mm inter-pebble gap was assumed. Pebble temperature profiles between the three stackings were investigated. It was concluded that the SC showed the highest fuel temperature among the three stackings. The model was evaluated for *Re* numbers between 1 and 5,000 based on Calis et al. [16] using a composite structure with *N*=1.

Wu et al. [23] used a BCC stacking with 28 pebbles and also modelled heat transfer within the pebbles with a RANS-based model. Pressure drops and temperature profiles were compared against a porous model approach [24]. Finally, *Nu* numbers and surface temperature profiles with respect to the zenith angle were investigated. Results were qualitatively similar to those of Lee et al. [19].

Dumas et al. [25] used 30×10 (identical to experiment) and 5×2 (periodic) pebbles, 'one-layer' staggered geometries. Pebbles were shrunk by 1% to avoid inter-pebble contact points. The wall shear stress of a pebble at Re=100 for both simulations were in good agreement with experimental data.

Yang et al. [26], based on Calis et al. [16] and Romkes et al. [17], initially, used a composite structure with N=1 to evaluate their model. This was then applied to a large number of regularly stacked beds. Pressure drops and Nu numbers were investigated.

Based on the above, it can be concluded that, numerical modelling of fluid flow and heat transfer through packed beds poses many challenges, especially with respect to mesh generation even when considering orderly stacked ones. In this study, a novel method for detailed modelling of physical processes in these complex geometries is proposed. The method is based on mesh adaptive LES and the implicit treatment of solid boundaries using a two-fluid approach. The resulting model is able to numerically resolve randomly packed beds along with areas of importance and/or interest starting off with arbitrarily coarse meshes. The main advantages of this method over existing ones are that the particle diameter does not need to be modified and more importantly any random packing regardless of inter-particle contact points can be modelled with minimal user meshing effort. A detailed review of similar methodologies can be found in Garcia et al. [27].

The model is, initially, evaluated using the composite structure proposed by Calis et al. [16] for N=1 and a range of Re numbers. The model is then applied to the FCC stacking as described in Lee and Lee [2, 3]. Coolant flow and heat transfer are investigated for both test cases.

The remainder of this paper is organised as follows. A detailed description of the model is given in Section 1. The model evaluation for the composite structure is presented in Section 2. The model application to the more realistic FCC packing is presented in Section 3. Finally, some concluding remarks and future work are given in Section 4.

1. **Governing equations**

The proposed approach is based on multi-fluid flow and thus, both the solid and the fluid are treated as fluids. The bulk velocity (u) is decomposed as $\mathbf{u} = \hat{\mathbf{u}}_f + \hat{\mathbf{u}}_s$, where $\hat{\mathbf{u}}_f = \alpha_f \mathbf{u}_f$ and $\hat{\mathbf{u}}_s = \alpha_s \mathbf{u}_s$. Subscripts s and f are used to denote the solid and fluid components, respectively. The volume fraction α is calculated using a conservative and bounded interpolation scheme [28].

The momentum equation for the fluid component is:

$$\rho_{f} \left(\frac{\partial \hat{\boldsymbol{u}}_{f}}{\partial t} + \boldsymbol{u}_{f} \cdot \nabla \hat{\boldsymbol{u}}_{f} \right) = -\nabla p + \nabla \cdot \boldsymbol{\tau} + \sigma_{f} (\hat{\boldsymbol{u}}_{s} - \boldsymbol{u}), \tag{1}$$
where ρ is the density, p is the perturbation pressure, $\boldsymbol{\tau}$ the viscous stress term and:
$$\sigma_{f} = \frac{\alpha_{s} \rho_{f}}{\Delta t} \tag{2}$$

$$\sigma_f = \frac{\alpha_s \rho_f}{\Delta t} \tag{2}$$

is a relaxation coefficient, where Δt is the time step size. The last term in Equation 1 is the integrated drag force per unit volume. The inverse time scale $(1/\Delta t)$ in Equation 2 is chosen so that the local bulk velocity is relaxed to the solid velocity in a time scale of one time step. The viscous stress term is:

$$\tau = (\mu + \mu_{\tau}) \cdot \nabla \hat{u}_f, \tag{3}$$

where μ is the fluid dynamic viscosity and μ_{τ} is the LES sub-grid scale viscosity calculated using an anisotropic Smagorinsky model [29]. The advantage of the model used here over the original Smagorinsky model is that the length scale is related directly to the local flow length scale, and varies in space, time and direction.

Assuming fluid and solid incompressibility, the combined continuity equation is:

$$\nabla \cdot \hat{\boldsymbol{u}}_{t} = 0. \tag{4}$$

Based on an approach similar to that taken for the fluid flow modelling, the bulk temperature (T) is decomposed as $T = \hat{T}_s + \hat{T}_f$ and heat transfer in the fluid component can be modelled using:

$$(\rho c_p)_f \left(\frac{\partial \hat{T}_f}{\partial t} + \mathbf{u}_{f'} \nabla \hat{T}_f \right) = \nabla \cdot \kappa_f \nabla \hat{T}_f + \sigma_f (\hat{T}_s - T), \tag{5}$$

where κ is the thermal conductivity and σ_f retains its previous meaning. Essentially, this formulation forces the temperature in the solid volume to a user-defined value (T_s) .

Nevertheless, in pebble bed reactor studies, using predefined volumetric heat sources, rather than temperatures or fluxes, is more appropriate. This can be modelled using:

$$(\alpha_{f}(\rho c_{p})_{f} + \alpha_{s}(\rho c_{p})_{s})(\frac{\partial T}{\partial t} + \mathbf{u}_{f} \nabla T) = \nabla \cdot (\alpha_{f} \kappa_{f} + \alpha_{s} \kappa_{s}) \nabla T + Q, \tag{6}$$

where Q is the volumetric heat source. On the solid-fluid interface the following boundary conditions have to be satisfied:

$$T_f = T_s \text{ and } \kappa_f \nabla T_f \cdot \boldsymbol{n} = \kappa_s \nabla T_s \cdot \boldsymbol{n},$$
 (7)

 $T_f = T_s$ and $\kappa_f \nabla T_f \cdot \boldsymbol{n} = \kappa_s \nabla T_s \cdot \boldsymbol{n}$, where \boldsymbol{n} is the solid-fluid interface outward-pointing normal unit vector.

The Navier-Stokes equations are discretised in space and time using the Bubnov-Galerkin finite element and Crank-Nicholson methods, respectively. The heat transfer equation is discretised using a high-order accurate control volume method based on total variation diminishing schemes. An integral part of this method is the anisotropic mesh adaptivity. This is based on the construction of a metric tensor field that is used to measure element edge lengths, and returns unit lengths for elements that are of the appropriate shape and size in metric space. The metric is built upon the Hessian matrix field for each solution component and predefined definitions of desired errors and incorporates maximum and minimum allowed edge lengths. These features have been implemented in a general purpose CFD model which in what follows is referred to as Fluidity. More details on the numerical methods used in Fluidity can be found in [30, 31]. More details on the implicit treatment of the solid boundaries can be found in [27].

2. Model evaluation using a composite structure

The model is evaluated using the composite structure proposed by Calis et al. [16] with N=1. Three simulations are undertaken with different Re numbers (1,000, 3,000 and 5,000), defined as: $Re=(u_{ref}/\varphi)d_h/v_f$, where φ is the porosity, $d_h=4\varphi/(1-\varphi)(V_s/A_s)_{cell}$ is the hydraulic diameter, v_f is the fluid kinematic viscosity and V_s and A_s are the unit cell solid volume and surface area, respectively. The dimensions of the unit cell are d_s^3 , where d_s is the pebble diameter. Each cell contains one whole pebble. The Pr number is 1. Heat transfer is modelled using Equation 5. The dimensions of the computational domain are $(L1+L2+L3)\times d_s\times d_s$, in the x, y and z directions,

respectively, where L1= $2.5d_s$, L2= $8d_s$ and L3= $6.67d_s$. The geometry includes 8 whole pebbles (and unit cells) within L2. A schematic of the computational domain is given in Figure 1.

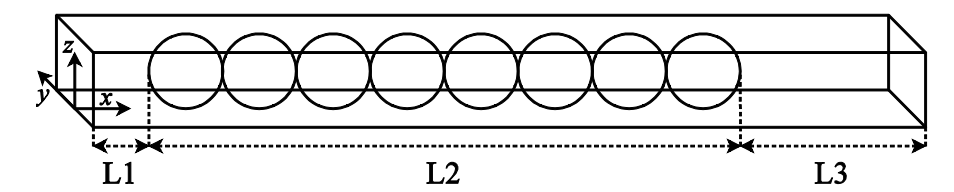


Figure 1 Schematic of the composite structure used to evaluate the proposed methodology.

Adaptive tetrahedral meshes with a maximum of 3,500,000 nodes are used. Element edge lengths in near-wall regions are constrained to $\approx 3y^+$ in the wall-normal direction, while in the cavities' cores they are $\approx 30y^+$, where y^+ is the distance from the wall in wall units defined as: $y^+=y$ u_τ/v_f and u_τ is the friction velocity. The transition from the finer regions to the coarser ones is smooth through the use of a linear gradation parameter in the mesh adaptivity algorithm. This ensures that adjacent element edge length differences do not exceed 30%. The mesh is adapted every 25 time steps. The adaptation is driven by the absolute interpolation error of the velocity, temperature and solid concentration fields. These are set to $0.05u_{\rm ref}$, $0.1T_{\rm ref}$ and 0.001, respectively (for more details see Pain et al. [31]). A sensitivity analysis based on the flow past a sphere in an infinite medium was undertaken to ensure mesh independent solutions. However, this is not presented here. An instantaneous diagonal cut plane of the mesh at $t^*=1.5$ for Re=1,000 is shown in Figure 2. The red colour represents the solid component, while the blue colour represents the fluid component. Time is non-dimensionalised using L2 and $u_{\rm ref}$.

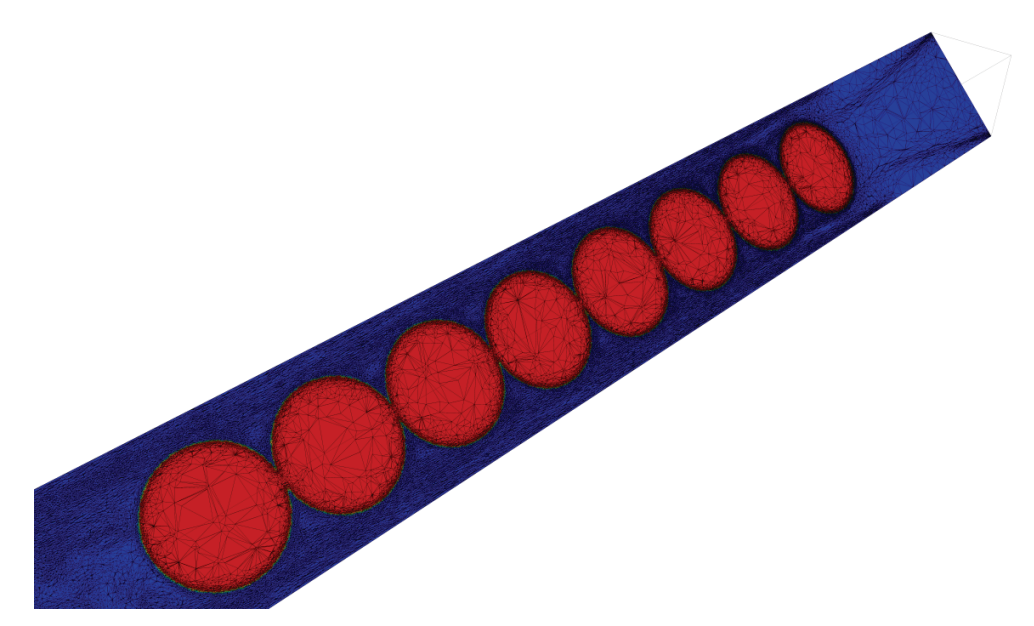


Figure 2 Instantaneous diagonal cut plane of the adapted mesh focused on the 8 pebbles at time $t^*=1.5$ for Re=1,000. The red colour represents the solid component, while the blue colour represents the fluid component (the flow is from the right).

A constant uniform velocity ($u=u_{ref}$) and temperature ($T=T_{ref}$) are applied on the inflow plane

(x=0). A no-slip boundary condition (u=0) along with a zero flux ($\nabla T \cdot \mathbf{n}$ =0) for temperature are applied on the channel walls (y= $\pm d_s/2$ and z=0, d_s), where \mathbf{n} is the channel boundary outward-pointing normal unit vector. Finally, a constant pressure is applied on the outflow plane (x=L1+L2+L3).

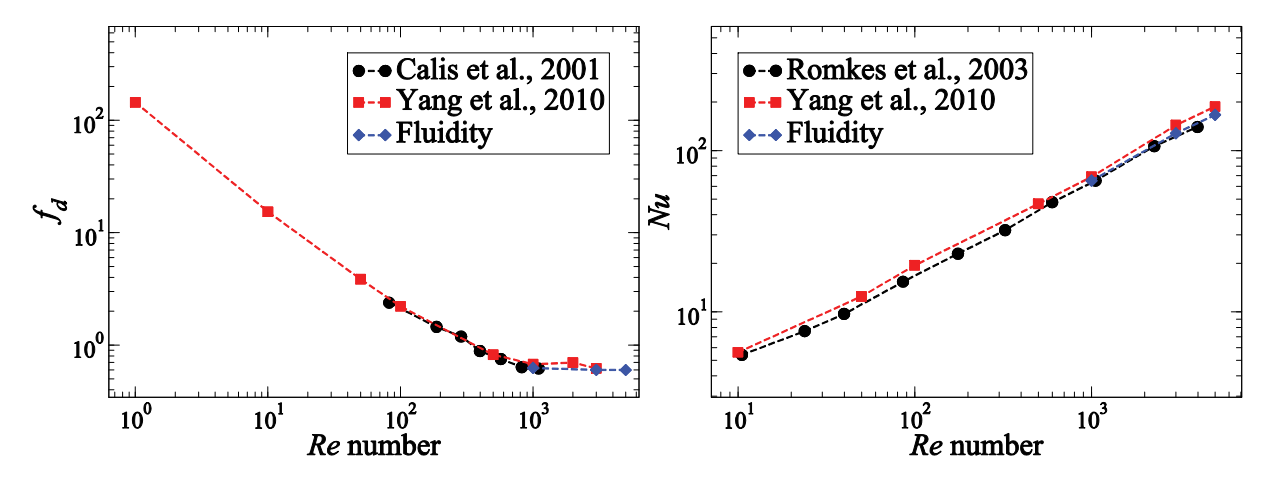


Figure 3 Comparison of friction factor and *Nu* number between the experimental data of Calis et al. [16] and Romkes et al. [17], the numerical simulations of Yang et al. [27] and Fluidity.

An adaptive time-stepping scheme is used to satisfy a maximum Courant-Friedrich-Lewy (CFL) number lower than unity. The averaging period for the data presented is 30 non-dimensional time units t^* after steady state has been reached. Linear interpolation is used to evenly distribute time for post-processing.

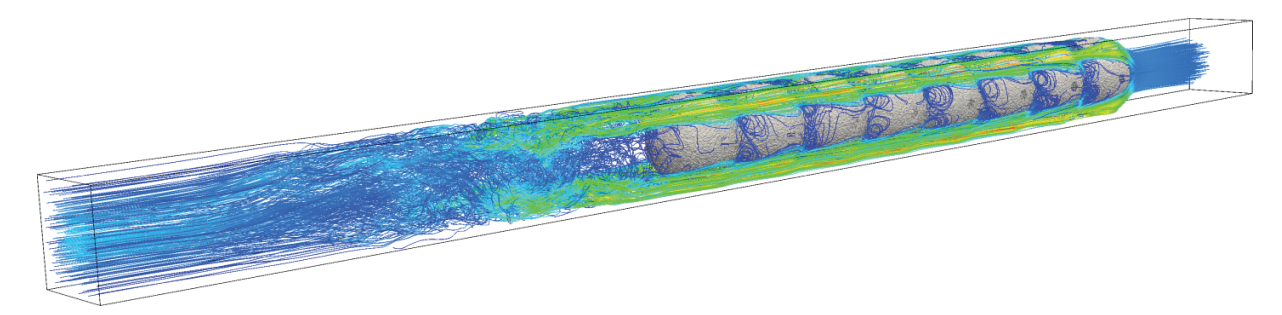


Figure 4 Instantaneous streamlines for Re=5,000 at time t*=1.5.

Diagnostics used for this evaluation include the friction factor (f_d) and Nu number. Based on Yang et al. [26], for this test case these are defined as:

$$f_d = 2\frac{d_h}{\rho_f} \left(\frac{\varphi}{u_{\text{ref}}}\right)^2 \frac{1}{3} \sum_{\text{cell}=5}^7 \frac{1}{(x_{\text{out}} - x_{\text{in}})A} \oint \left(p_{\text{in}} - p_{\text{out}}\right) dA \text{ and } Nu = \frac{d_s}{\kappa_f} \frac{1}{3} \sum_{\text{cell}=5}^7 \frac{(\rho c_p)_f \oint \mathbf{u} \cdot \mathbf{n} (T_{\text{out}} - T_{\text{in}}) dA}{A_s (T_s - \overline{T}_f)}$$
(8)

where, x are the Cartesian coordinates in the flow direction, subscripts in and out denote the inflow and outflow of each unit cell, respectively, A is the unit cell inflow/outflow surface area and $\overline{T}_f = 0.5 \oint u \cdot n(T_{\text{out}} + T_{\text{in}}) dA / \oint u \cdot n dA$ is the average fluid temperature in the unit cell. Unit cell inflow/outflow surface integrals are evaluated on 100×100 uniform grids. Note that f_d and Nu are evaluated over cells 5, 6 and 7 only.

The 14th International Topical Meeting on Nuclear Reactor Thermalhydraulics, NURETH-14 Toronto, Ontario, Canada, September 25-30, 2011

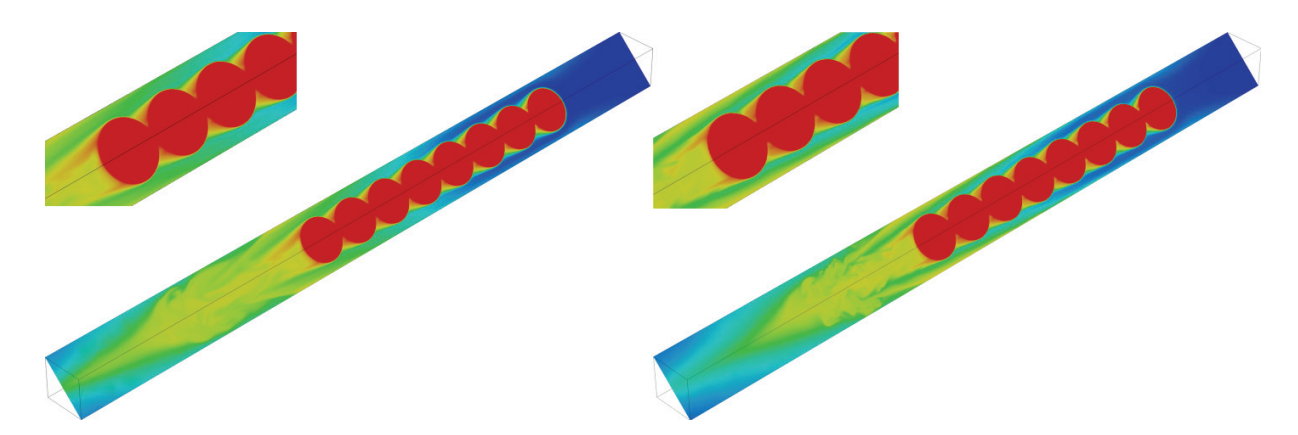


Figure 5 Instantaneous diagonal cut planes of the domain and magnification of the 4 pebbles near the outflow for the temperature field at time $t^*=1.5$. Left: Re=1,000. Right: Re=5,000 (the flow comes from the right).

Comparison between the experimental data of Calis et al. [16] and Romkes et al. [17], the numerical simulations of Yang et al. [26] and Fluidity is given in Figure 3. Fluidity is in good agreement with the reference data for both the friction factor and the Nu number. 400 instantaneous streamlines for Re=5,000 at time $t^*=1.5$ are shown in Figure 4. They originate from a sphere of radius $r_s=3d_s/4$ and centre (L1/4, 0, $d_s/2$). Paths are calculated using a fourth-order, forward, Runge-Kutta method. High velocity zones adjacent to the channel edges and recirculation zones between pebbles are evident. These recirculation zones lead to poor heat transfer and can be responsible for the emergence of hot-spots. Instantaneous diagonal cut planes for the temperature field for Re=1,000 and 5,000 at time $t^*=1.5$ are shown in Figure 5. The lower temperatures in the high velocity areas and the higher temperatures in the recirculation areas are evident for both cases. Comparing the two temperature patterns it becomes apparent that the hot-spots become stronger with increasing Re number, especially between pebbles close to the outflow. Finally, the turbulent structures in the wake of the bed are smaller and the boundary laver is thinner, for the high Re case.

3. Model application to the FCC stacking

The model is applied to the scaled-up FCC packing as described in Lee and Lee [2, 3]. The Re number, defined as: $Re=u_{ref}d_n/v_f$, is 10,807. Apart from the Re number all other material properties used in the heat transfer equation (Equation 6) are based on the 400MWth PBMR [32] near the outflow. An 850°C inflow temperature (T_{ref}) and 9MPa operating pressure are assumed. Pebbles are assumed to consist of graphite only and the coolant used is He. Based on the DIREKT manual [33]: ρ_f =3.82kg/m³, c_{pf} =5195J/(kgK), κ_f =0.395W/(mK), ρ_s =1750kg/m³, c_{ps} =1873.443J/(kgK) and κ_s =14.866W/(mK). These values are then scaled to reflect the modified Re number and scaled-up pebble diameter (d_s) of 12cm. The Pr number is 0.64. The dimensions of the computational domain are (L1+L2+L3)×17×17cm³, in the x, y and z directions, respectively, where L1=9, L2=29 and L3=60cm. Segment L3 is longer than it is in the wind tunnel experiments in order to avoid outflow boundary effects. The geometry includes 6 pebbles (2 whole, 4 half and 8 quarter pebbles) within L2. L1, L2 and L3 retain their previous meaning and represent the flow development, porous and outflow area lengths, respectively. A two-dimensional schematic of the computational domain along with the geometry's cavity (shaded area) to be investigated is given in Figure 6.

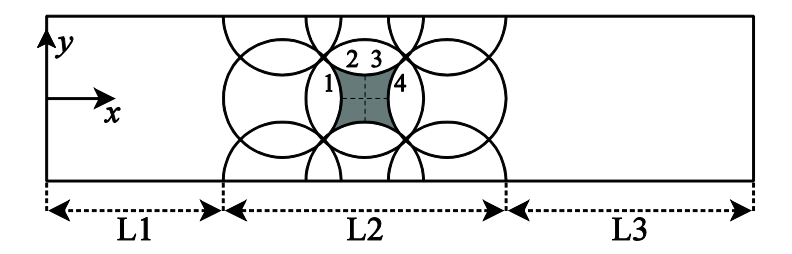


Figure 6 Two-dimensional schematic of the FCC stacking.

Mesh adaptivity parameters, boundary conditions and time-stepping options are identical to those in Section 2 and are not repeated here. The pebble fuel (inner) zone (with a radius of 5cm) temperature field is initialised based on the analytical solution of the Poisson equation for a constant boundary temperature. As far as the volumetric heat source (*Q* in Equation 6) is concerned, a uniform heat source is applied on the fuel zone of all pebbles in the domain.

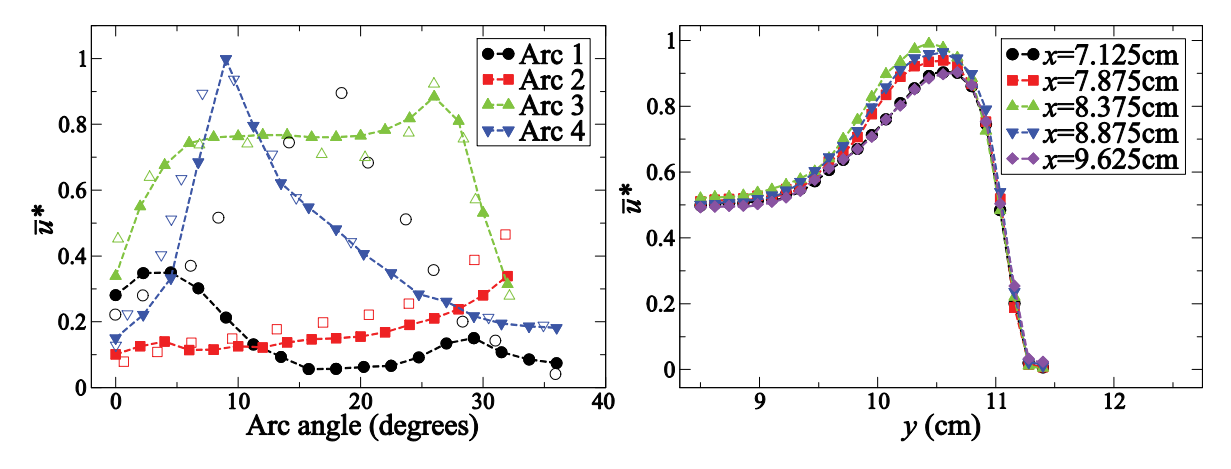


Figure 7 Normalised time-averaged velocity magnitude profiles on the symmetry plane (*z*=8.5cm) of the geometry's central cavity. Left: 4 arcs 1.5mm away from the pebble wall. Hollow symbols: Lee and Lee [3], Solid symbols: Fluidity. Right: 5 lines perpendicular to the flow direction.

The normalised time-averaged velocity magnitude, defined as: $\bar{u}^*=c(u^2+v^2+w^2)^{1/2}$, where c=1/1.75, on the symmetry plane (z=8.5cm) of the geometry's central cavity 1.5mm away from the pebble boundary is shown in Figure 7 (left). The 4 36° arcs used start from (L1+ d_s , 8.5cm, 8.5cm) and finish at (L1+L2- d_s , 8.5cm, 8.5cm). Therefore, Arc 1 is on the lee side, Arc 4 is on the windward side and Arcs 2 and 3 are in between. The 4 arcs are also shown in Figure 5. Angularly evenly distributed points are used for these profiles. Hereafter, θ is used to denote the arc angle and $\theta=0^\circ$ at the start point of each arc. Bold symbols correspond to the numerical simulation and hollow symbols correspond to the physical simulation. Wind tunnel data were compiled by digitising and averaging results presented in Lee and Lee [3]. Arc 1 gives two small peaks at $\theta\approx4$ and 30°. Arc 2 gives a small peak at $\theta\approx4^\circ$ and then the velocity magnitude steadily increases. In Arc 3 the velocity continues to increase until $\theta\approx26^\circ$ and then decreases rapidly as the inter-pebble contact point is approached. Finally, in Arc 4 the velocity increases rapidly until $\theta\approx9^\circ$ and then decreases. Both models give similar velocity patterns with the exception of Arc 1, where the wind tunnel data give a large peak at $\theta\approx20^\circ$.

The normalised time-averaged velocity magnitude, with c=1/2, on the symmetry plane (z=8.5cm) of the geometry's central cavity for 5 different profiles (x=9.625, 8.875, 8.375, 7.875 and 7.125cm) for y=(L1+L2/2, L1+L2/2+2.5cm) is shown in Figure 7 (right). 25 evenly distributed points are used for each profile. Velocity magnitudes are normalised. All profiles give a peak at a distance of \approx 0.5-1.5cm from the pebble wall and then the velocity magnitude decreases with increasing distance from the wall. This is caused by the cavity upwind and downwind blockage of the FCC stacking. In addition, the peak magnitude slightly increases for profiles closer to the centre of the cavity.

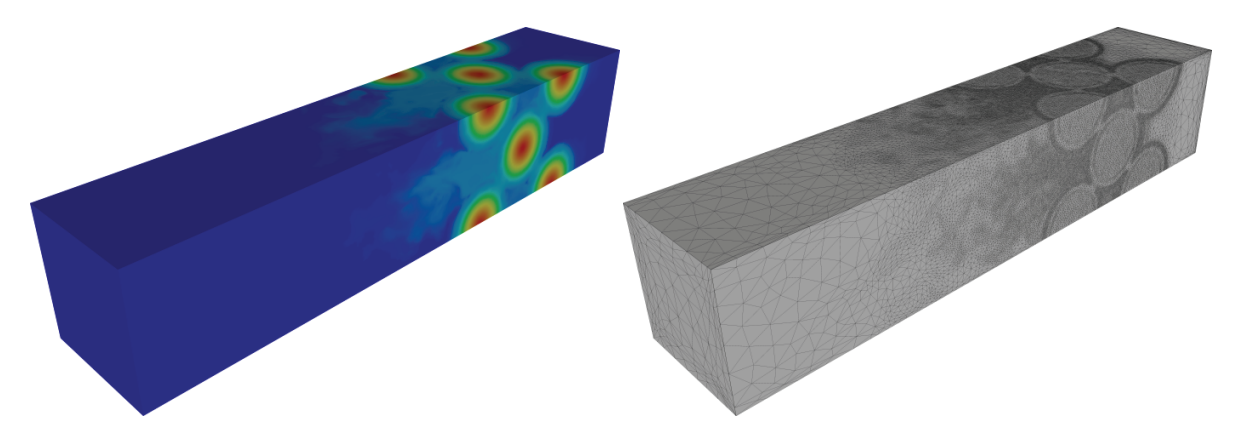


Figure 8 Instantaneous temperature field along with the adapted surface mesh at time t*=1.5 (the flow comes from the right).

The instantaneous temperature field on the computational domain boundaries along with the adapted surface mesh at time $t^*=1.5$ are shown in Figure 8.

4. Conclusions

A novel method for simulating coolant flow and heat transfer in pebble bed reactors has been presented. The method is based on mesh adaptive LES and implicit treatment of solid boundaries. The resulting model is able to numerically resolve randomly packed beds along with areas of importance and/or interest starting off with arbitrarily coarse meshes. The main advantages of this method over existing ones are that the particle diameter does not need to be modified and more importantly any random packing regardless of inter-particle contact points can be modelled with minimal user meshing effort.

The model was evaluated using the composite structure proposed by Calis et al. [16] with N=1 for Re numbers between 1,000 and 5,000. It was able to accurately reproduce the bed geometry by refining the mesh on the implicit boundaries and flow recirculation areas, while minimising the computation cost by coarsening the mesh within the solids where the temperature was fixed. Friction factors and Nu numbers were in good agreement with the reference experimental and numerical data.

The model was then applied to the more realistic FCC stacking as described in Lee and Lee [2, 3]. It was able to accurately reproduce the bed geometry by refining the mesh on the implicit boundaries and flow recirculation areas, but this time the mesh was also refined within the pebbles in order to model heat transfer within the solids. Coolant flow and temperature patterns

were investigated. Coolant flow patterns were qualitatively comparable to the reference data.

Taken together, the results presented here have established with sufficient confidence that the model can be used to successfully and efficiently simulate coolant flow and heat transfer in pebble bed reactors. Future work includes application of the model to stochastically generated beds with a view to assessing and improving macroscopic models.

5. References

- [1] Y.A. Hassan and E.E. Dominguez-Ontiveros, "Flow visualization in a pebble bed reactor experiment using PIV and refractive index matching techniques", *Nuclear Engineering and Design*, Vol. 238, 2008, pp. 3080-3085.
- [2] J.-Y. Lee and S.-Y. Lee, "Flow visualization in the scaled up pebble bed of high temperature gas-cooled reactor using particle image velocimetry method", *Journal of Engineering for Gas Turbines and Power*, Vol. 131, 2009, No. 064502.
- [3] J.-Y. Lee and S.-Y. Lee, "Flow visualization of pebble bed HTGR". <u>Proceedings of the 4th International Topical Meeting on High Temperature Reactor Technology (HTR2008)</u>, Washington DC, USA, 2008 September 28-October 1.
- [4] M.T. Dalman, J.H. Merkin and C. McGreavy, "Fluid flow and heat transfer past two spheres in a cylindrical tube", *Computers & Fluids*, Vol. 14, 1986, pp. 267-281.
- [5] F. Kuwahara, A. Nakayama and H. Koyama, "A numerical study of thermal dispersion in porous media", *Journal of Heat Transfer*, Vol. 118, 1996, pp. 756-761.
- [6] F. Kuwahara and A. Nakayama, "Numerical determination of thermal dispersion coefficients using a periodic porous structure", *Journal of Heat Transfer*, Vol. 121, 1999, pp. 160-163.
- [7] F. Kuwahara M. Shirota and A. Nakayama, "A numerical study of interfacial convective heat transfer coefficient in two-energy equation model for convection in porous media", *International Journal of Heat and Mass Transfer*, Vol. 44, 2001, pp. 1153-1159.
- [8] M.H.J. Pedras and M.J.S. de Lemos, "Simulation of turbulent flow in porous media using a spatially periodic array and a low Re two-equation closure", *Numerical Heat Transfer, Part A: Applications*, Vol. 39, 2001, pp. 35-59.
- [9] A. Nakayama and F. Kuwahara, "A general macroscopic turbulence model for flows in packed beds, channels, pipes, and rod bundles", *Journal of Fluids Engineering*, Vol. 130, 2008, No. 101205.
- [10] J. Tobiś, "Influence of bed geometry on its frictional resistance under turbulent flow conditions". *Chemical Engineering Science*, Vol. 55, 2000, pp. 5359-5366.
- [11] P.R. Gunjal, V.V. Ranade and R.V. Chaudhari, "Computational study of a single-phase flow in packed beds of spheres", *American Institute of Chemical Engineers Journal*, Vol. 51, 2005, pp. 365-378.
- [12] S.A. Logtenberg and A.G. Dixon, "Computational fluid dynamics studies of fixed bed heat transfer", *Chemical Engineering and Processing*, Vol. 37, pp. 1998 7-21.
- [13] S.A. Logtenberg, M. Nijemeisland and A.G. Dixon, "Computational fluid dynamics simulations of fluid flow and heat transfer at the wall-particle contact points in a fixed-bed reactor", *Chemical Engineering Science*, Vol. 54, 1999, pp. 2433-2439.
- [14] M. Nijemeisland and A.G. Dixon, "Comparison of CFD simulations to experiment for convective heat transfer in a gas–solid fixed bed", *Chemical Engineering Journal*, Vol. 82, 2001, pp. 231-246.

- [15] A.G. Dixon and M. Nijemeisland, "CFD as a design tool for fixed-bed reactors", *Industrial & Engineering Chemistry Research*, Vol. 40, 2001, pp. 5246-5254.
- [16] H.P.A. Calis, J. Nijenhuis, B.C. Paikert, F.M. Dautzenberg and C.M. van den Bleek, "CFD modelling and experimental validation of pressure drop and flow profile in a novel structured catalytic reactor packing", *Chemical Engineering Science*, Vol. 56, 2001, pp. 1713-1720.
- [17] S.J.P. Romkes, F.M. Dautzenberg, C.M. van den Bleek and H.P.A. Calis, "CFD modelling and experimental validation of particle-to-fluid mass and heat transfer in a packed bed at very low channel to particle diameter ratio", *Chemical Engineering Journal*, Vol. 96, 2003, pp. 3-13.
- [18] A. Guardo, M. Coussirat, M. Angels Larrayoz, F. Recasens and E. Egusquiza, "CFD flow and heat transfer in nonregular packings for fixed bed equipment design", *Industrial & Engineering Chemistry Research*, Vol. 43, 2004, pp. 7049-7056.
- [19] J.-J. Lee, G.-C. Park, K.-Y. Kim and W.-J. Lee, "Numerical treatment of pebble contact in the flow and heat transfer analysis of a pebble bed reactor core", *Nuclear Engineering and Design*, Vol. 237, 2007, pp. 2183-2196.
- [20] J.-J. Lee, S.-J. Yoon, G.-C. Park and W.-J. Lee, "Turbulence-induced heat transfer in PBMR core using LES and RANS", *Journal of Nuclear Science and Technology*, Vol. 44, 2007, pp. 985-996.
- [21] Y.A. Hassan, "Large eddy simulation in pebble bed gas cooled core reactors", *Nuclear Engineering and Design*, Vol. 238, 2008, pp. 530-537.
- [22] M.-H. Kim, H.-S. Lim and W.J. Lee, "Computational fluid dynamics assessment of the local hot core temperature in a pebble-bed type very high temperature reactor", *Journal of Engineering for Gas Turbines and Power*, Vol. 131, 2009, No. 012905.
- [23] C.Y. Wu, Y.M. Ferng, C.C. Chieng and C.C. Liu, "Investigating the advantages and disadvantages of realistic approach and porous approach for closely packed pebbles in CFD simulation". *Nuclear Engineering and Design*, Vol. 240, 2010, pp. 1151-1159.
- [24] W.J. van Rooyen, D.L.W. Krueger, E.H. Mathews and M. Kleingeld, "Simulation and optimisation of gas storage tanks filled with heat sink". *Nuclear Engineering and Design*, Vol. 226, 2006, pp. 156-163.
- [25] T. Dumas, F. Lesage and M.A. Latifi, "Modelling and measurements of the velocity gradient and local flow direction at the pore scale of a packed bed", *Chemical Engineering Research and Design*, Vol. 88, 2010, pp. 379-384.
- [26] J. Yang, Q. Wang, M. Zeng and A. Nakayama, "Computational study of forced convective heat transfer in structured packed beds with spherical or ellipsoidal particles". *Chemical Engineering Science*, Vol. 65, 2010, pp. 726-738.
- [27] X. Garcia, D. Pavlidis, G.J. Gorman, J.L.M.A. Gomes, M.D. Piggott, E Aristodemou, J. Mindel, J.-P. Latham, C.C. Pain, H. ApSimon, "A two-phase adaptive finite element method for solid-fluid coupling in complex geometries", *International Journal for Numerical Methods in Fluids*, Vol. 66, 2011, pp. 82-96.
- [28] P.E. Farrell, M.D. Piggott, C.C. Pain, G.J. Gorman, C.R. Wilson, "Conservative interpolation between unstructured meshes via supermesh construction", *Computer Methods in Applied Mechanics and Engineering*, Vol. 198, 2009, pp. 2632-2642.
- [29] E. Aristodemou, T. Bentham, C. Pain, R. Colvile, A. Robins and H. ApSimon, "A comparison of mesh-adaptive LES with wind tunnel data for flow past buildings: Mean flows and velocity fluctuations", *Atmospheric Environment*, Vol. 43, 2009, pp. 6238-

6253.

- [30] R. Ford, C.C. Pain, M.D. Piggott, A.J.H. Goddard, C.R.E. de Oliveira and A.P. Umpleby, "A nonhydrostatic finite-element model for three-dimensional stratified oceanic flows. Part I: Model formulation", *Monthly Weather Review*, Vol. 132, 2004, pp. 2816-2831.
- [31] C.C. Pain, A.P. Umpleby, C.R.E. de Oliveira and A.J.H. Goddard, "Tetrahedral mesh optimisation and adaptivity for steady-state and transient finite element calculations", *Computer Methods in Applied Mechanics and Engineering*, Vol. 190, 2001, pp. 3771-3796
- [32] A. Koster, H.D. Matzner and D.R. Nicholsi, "PBMR design for the future", *Nuclear Engineering and Design*, Vol. 22, 2003, pp. 231-245.
- [33] S. Struth, "DIREKT input description", FZ Jülich, Germany, 2008, pp. 72.